SCIENTIFIC REP⚙RTS

OPEN

Magnetization Reversal by Out-of-plane Voltage in BiFeO$_3$-based Multiferroic Heterostructures

J. J. Wang[1,*], J.M. Hu[1,2,*], Ren-Ci Peng[1], Y. Gao[1], Y. Shen[1], L. Q. Chen[1,2] & C. W. Nan[1]

Voltage controlled 180° magnetization reversal has been achieved in BiFeO3-based multiferroic heterostructures, which is promising for the future development of low-power spintronic devices. However, all existing reports involve the use of an in-plane voltage that is unfavorable for practical device applications. Here, we investigate, using phase-field simulations, the out-of-plane (i.e., perpendicular to heterostructures) voltage controlled magnetism in heterostructures consisting of CoFe nanodots and (110) BiFeO$_3$ thin film or island. It is predicted that the in-plane component of the canted magnetic moment at the CoFe/BiFeO$_3$ interface can be reversed repeatedly by applying a perpendicular voltage across the bottom (110) BiFeO$_3$ thin film, which further leads to an in-plane magnetization reversal in the overlaying CoFe nanodot. The non-volatility of such perpendicular voltage controlled magnetization reversal can be achieved by etching the continuous BiFeO$_3$ film into isolated nanoislands with the same in-plane sizes as the CoFe nanodot. The findings would provide general guidelines for future experimental and engineering efforts on developing the electric-field controlled spintronic devices with BiFeO$_3$-based multiferroic heterostructures.

Multiferroic magnetoelectric (ME) heterostructures are comprised of at least two different ferroic (ferromagnetic, ferroelectric, antiferromagnetic, etc.) materials that are artificially combined with well-defined interface[1–5]. In multiferroic ME heterostructures, the ability to switch magnetization directly using an electric voltage rather than electric current (i.e., magnetoelectric coupling) can potentially be implemented to solve the overheating problem in spintronic devices[6–8]. Among the various multiferroic ME heterostructures, the magnet/BiFeO$_3$ (BFO) heterostructure is attracting increasing research efforts[9–18], in which the ferroelectric (FE) polarization **P** is coupled to the magnetization **M** in the overlaying magnet, based on the intrinsic room-temperature ME coupling between **P** and the antiferromagnetic axis **L** in the BFO, and the exchange coupling between **M** and **L**. In particular, in Co$_{90}$Fe$_{10}$ (abbreviated to CoFe)/BFO thin-film heterostructures, voltage controlled net magnetization reversal has been demonstrated driven by this interfacial exchange interaction[10,13]. A voltage controlled uniform (i.e., magnetic single-domain) magnetization reversal is further predicted under the action of both exchange interaction and ferroelastic strain[16]. However, in these CoFe/BFO heterostructures, the voltage was applied through in-plane electrodes grown on top of the BFO film[10,13]. These in-plane electrode configuration introduces unfavorable factors including too large coercive voltage, too large size limitation, and inconvenient integration into conventional microelectronics circuits. Therefore, an out-of-plane (i.e., perpendicular) voltage configuration across the BFO film is highly desired, for the design of high-performance spintronic devices[19,20]. Soon after we submitted the present article, a wonderful experimental work on the magnetization reversal by out-of-plane voltage in the CoFe/(110) BFO heterostructure was reported[21], further indicating this future research tendency in the BFO-based multiferroic heterostructures. In this article, we demonstrate,

[1]State Key Lab of New Ceramics and Fine Processing, School of Materials Science and Engineering, Tsinghua University, Beijing, 100084, China. [2]Department of Materials Science and Engineering, The Pennsylvania State University, University Park, Pennsylvania, 16802, USA. *These authors contributed equally to this work. Correspondence and requests for materials should be addressed to C.W.N. (email: cwnan@tsinghua.edu.cn)
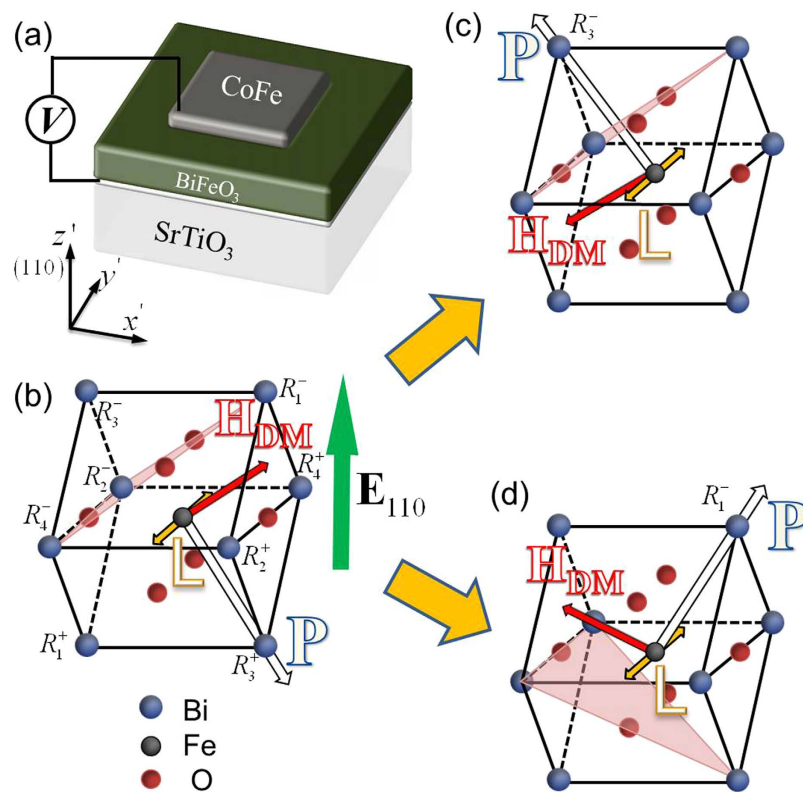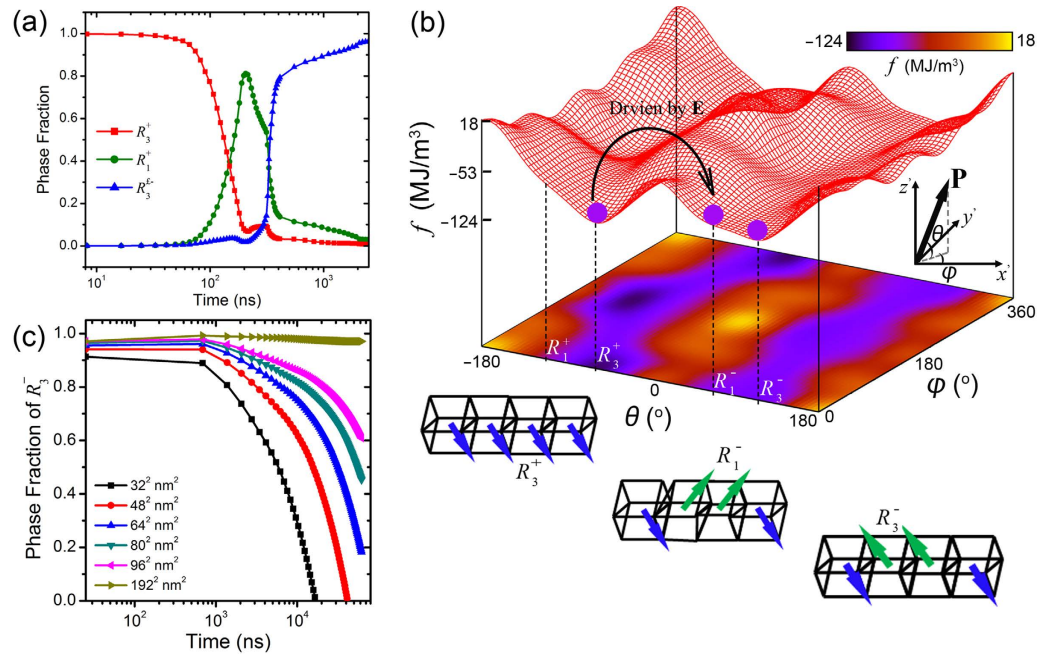
Figure 1. Voltage-induced ferroelectric and antiferromagnetic switching in CoFe/(110) BiFeO$_3$ heterostructure. (a) Schematic illustration of the proposed CoFe/(110) BiFeO$_3$ multiferroic heterostructure under perpendicular voltage modulation. **(b)** The lattice structures of (110) BiFeO$_3$ film in R_3^+ phase, and under perpendicular electric field along [110] direction, the polarization may switch by **(c)** 180° to R_3^- phase, or **(d)** 109° to R_1^- phase.

using phase field method[16,22,23], a mesoscale morphological engineering approach to achieving perpendicular voltage controlled magnetization reversal in magnetic/BFO thin-film heterostructures.

Consider the widely investigated Co$_{90}$Fe$_{10}$ (abbreviated to CoFe herein)/BFO heterostructure as an example. Compared to the (001)-oriented BFO films in previous CoFe/BFO heterostructures[10,13,16], a (110)-oriented BFO film is utilized herein, which can be grown on a (110) SrTiO$_3$ substrate with SrRuO$_3$ as the bottom electrode[24]. An electric voltage is then applied perpendicularly through the SrRuO$_3$ and the top CoFe dot that can be cut out from a continuous CoFe film by focused ion beams[25], as shown in Fig. 1a. In order to demonstrate the perpendicular voltage-induced magnetization reversal, a phase field model is developed to understand and predict the switching behaviors of the polarization and magnetization in the (110) BFO thin film/island and the CoFe dot (see Methods).

Results

Principles of the Perpendicular Voltage Controlled Magnetization Reversal.
By engineering the substrate[26,27] or pre-poling[24] the (110) BFO film using piezoelectric force microscopy (PFM) before sputtering the CoFe layer, remnant polarization distributions with single-domain state or large surface-area (usually larger than 3 μm × 3 μm) individual domains can be obtained according to experiments[24,26,27]. Therefore, it is very likely that the patterned nanoscale CoFe dot lies on an individual domain of BFO with much larger size over microns, for instance, the R_3^+ domain with **P** along $[\bar{1}\bar{1}1]$ as shown in Fig. 1a. Given that the polarization **P**, the antiferromagnetic axis **L**, and the canted magnetic moment **M**$_{cant}$ induced via the Dzyaloshinskii-Moriya (DM) interaction[28,29] (the contribution of which can be described by an effective magnetic field **H**$_{DM}$ along the same direction) are orthogonal to each other[30,31] at the CoFe/BFO interface, i.e., **M**$_{cant}$ (**H**$_{DM}$) = **P** × **L**[13,32], and also given that **L** is along the $[\bar{1}10]$ direction for the R_3^+ (i.e., **P**→$[\bar{1}\bar{1}1]_c$) domain according to experimental observations[33], the **H**$_{DM}$ field should be along the $[20\sqrt{2}]_{x'}$ direction. Under a negative perpendicular voltage applied along the [110] direction between the SrRuO$_3$ and CoFe electrodes, the polarization may either switch by 180° from R_3^+ to R_3^- (i.e., **P**→$[11\bar{1}]_c$) (Fig. 1c) or by 109° from R_3^+ to R_1^- (i.e., **P**→$[111]_c$) (Fig. 1d). Experiments also show that the antiferromagnetic axis **L** along $[\bar{1}10]$ does not rotate[30] for both switching paths, though the antiferromagnetic plane rotates during the 109° switching[33]. As a result, the **H**$_{DM}$ field rotates from $[20\sqrt{2}]_{x'}$ to $[\bar{2}0\sqrt{2}]_{x'}$ or

2

Figure 2. Mechanism of voltage-induced 180° ferroelectric switching in CoFe /(110) BiFeO$_3$ heterostructure. For (110) BiFeO$_3$ thin film with 80×80 nm^2 CoFe dots grown above as the top electrode and ferromagnetic layer, the [110] electric field induced (**a**) phase evolutions and (**b**) the switching path R_3^+ from first to R_1^- and then to R_3^-, obtained from the total energy profile as a function of polarization orientation defined by θ and ϕ in inset schematic coordinate system. The total energy in (**b**) is illustrated by both the 3-Dimensional grid curves and 2-Dimensional color contour map. The inset lattice structures illustrate the polarization orientation of R_3^+, R_1^- and R_3^- phase (i.e., $\mathbf{P} \rightarrow [\bar{1}\bar{1}1]_c$ for R_3^+, $\mathbf{P} \rightarrow [111]_c$ for R_1^-, and $\mathbf{P} \rightarrow [11\bar{1}]_c$ for R_3^-, see Fig. 1). (**c**) Phase evolutions of R_3^- after removing the voltage for CoFe/(110)-film BiFeO$_3$ multiferroic heterostructures with different CoFe size.

$[\bar{2}0\overline{\sqrt{2}}]_{x'}$ after the 109° or 180° switching, respectively. Such reversal of the in-plane component of $\mathbf{H}_{DM}$ field may further induce a reversal of in-plane net magnetization as demonstrated later. If the CoFe nanodot does not lie on an individual domain but on the domain wall of BFO, the electric field control of magnetization would be weakened because the interfacial exchange coupling can be neutralized due to the inhomogeneity of the polarization as well as the DM field at the BFO domain wall.

Features of polarization/magnetization reversal in CoFe dot /(110) BFO film and island.   As shown in Fig. 2a, by applying a negative voltage (i.e., with upward electric fields) of $-2V_c$ (V_c being the coercive voltage) across the (110) BFO film through the CoFe dot with an in-plane size of 80 nm $\times$ 80 nm and SrRuO$_3$ bottom electrode, the volume fraction of R_3^+ domain in the region underneath the CoFe drops dramatically after about 5 ns. Meanwhile, the volume fraction of R_1^- domain increases greatly and reaches a maximum value of 81% (with respect to the poled region) after about 200 ns and then decreases rapidly. This is accompanied by the dramatic increase in the volume fraction of R_3^- domain. After 1500 ns, the polarizations underneath the CoFe dot are stabilized almost as a R_3^- single-domain with a volume fraction of 96.3%. This sub-μs ferroelectric switching time is consistent with experimental observations in BiFeO$_3$ and Pb(Zr,Ti)O$_3$ films[34,35]. Such polarization reversal via successive 109° switching from R_3^+ to R_1^- and 71° switching from R_1^- to R_3^- under perpendicular voltage has been experimentally observed in (110) and (001) BFO films[24,36].

To understand the underlying physics for this ferroelectric switching path, we calculate the total free energy density profile by setting the polarization in the region underneath the CoFe dot of 192 nm $\times$ 192 nm pointing along every directions (see the orientation angles θ and ϕ) in the $x'y'z'$ coordinate system. As shown in Fig. 2b, for an initial R_3^+ domain, the low-energy polarization switching path is within the $R_1^+R_3^+R_1^-R_3^-$ plane ($\phi = 0°$). An electric field along [110] direction is required to overcome the energy barrier, which mainly results from the elastic and Landau-type bulk free energy, to switch the R_3^+ domain ($\theta = -58°$, $\phi = 0°$) to the metastable (see the saddle point in the energy density profile) R_1^- ($\theta = 70°$, $\phi = 0°$), which would further relax to the R_3^- ($\theta = 112°$, $\phi = 0°$) domain. Although the electric energy increases as the head to tail R_3^+(unpoled region)/R_1^- (poled region) 109°domain wall changes into the R_3^+/R_3^- domain wall during the latter process, the elastic energy decreases more significantly. Indeed, when
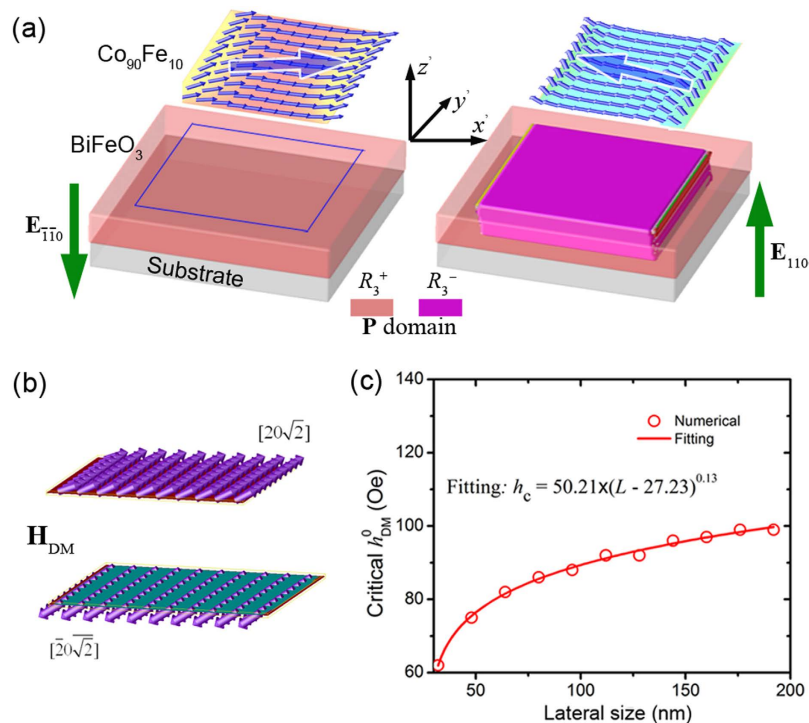
Figure 3. Voltage-controlled magnetism in CoFe/(110) BiFeO₃ heterostructure. (**a**) Perpendicular electric field induced ferroelectric and ferromagnetic domains switching in dot CoFe/(110)-thin-film BFO multiferroic heterostructure mediated by (**b**) the interfacial DM fields. (**c**) Dependence of the critical DM field strength which can make the net magnetization switch 150° under perpendicular voltage on the in-plane lateral size (length and width) of CoFe dots.

the polarization underneath the CoFe dot is R_3^+, R_1^- and R_3^-, the corresponding elastic and electric energy densities ($f_{elastic}$, $f_{electric}$) are (6.91 MJ/m³, −4.01 MJ/m³), (14.1 MJ/m³, −4.18 MJ/m³), and (5.97 MJ/m³, 2.64 MJ/m³), respectively.

Figure 2c further shows the time-dependent evolution of the R_3^- domain volume fraction in the BFO region underneath the CoFe electrode after removing the negative voltage of $-2V_c$, with the in-plane size of the CoFe dot varying from 32 nm × 32 nm to 192 nm × 192 nm. Once removing the voltage, the R_3^+/R_3^- multi-domain will evolve back to the R_3^+ single-domain to reduce the electric energy, which is evidenced by the presence of global energy minima at the R_3^+ single-domain in the profile shown in Fig. 2b. Such relaxation of high-energy domain structure has been experimentally observed in BFO thin films[36,37]. Nevertheless, the stability of the R_3^+/R_3^- multi-domain can be improved by increasing the in-plane size of the CoFe electrode (e.g., to 192 nm × 192 nm), as shown in Fig. 2c.

Now turn to discuss how the perpendicular electric field modulates the magnetization distribution in CoFe dots through the interfacial exchange interaction mechanism. As discussed above, the (110) BFO thin film can be pre-poled to become a single domain over a micron scale range, for instance, the R_3^+ single domain obtained by applying a positive voltage along [$\bar{1}\bar{1}0$] direction (see Fig. 3a). In this case, the magnetization distribution in the CoFe dot of 192 nm × 192 nm × 2.5 nm exhibits a typical 'leaf'-like ground state structure[38] with average magnetization component $m_{x'} = 0.90$, $m_{y'} = 0.31$ under the interface $\mathbf{H}_{DM}$ field along the $[20\sqrt{2}]_{x'}$ direction (see the top part of Fig. 3b). As the electric field reverses to be along [110] direction under negative voltages (on the right of Fig. 3a), the local R_3^+ domain in the region underneath the CoFe dot transforms into a local R_3^- domain by successive 109° and 71° switching, leading to a reoriented interface $\mathbf{H}_{DM}$ field along the $[\bar{2}0\sqrt{2}]_{x'}$ direction (see the bottom part of Fig. 3b). Accordingly, the average magnetization components gradually changes to $m_{x'} = -0.90$, $m_{y'} = 0.31$, i.e., it occurs a 150° reversal of the net magnetization along the in-plane x' axis. Note that such reversal of in-plane net magnetization requires a sufficiently large magnitude of the interface $\mathbf{H}_{DM}$ field (namely, h_{DM}^0). The critical value of h_{DM}^0 is dependent on the in-plane size of the CoFe dot. As shown in Fig. 3c, the critical h_{DM}^0 value increases with increasing in-plane lateral size L (the length and width being the same) as a power-function. Specifically, for the CoFe dots with in-plane size below 192 nm × 192 nm, the critical h_{DM}^0 value is about 100 Oe, quite close to the experimentally measured value (about 100 Oe) in a similar layered heterostructure of polycrystalline CoFe thin film and (001) BFO thin films[15].
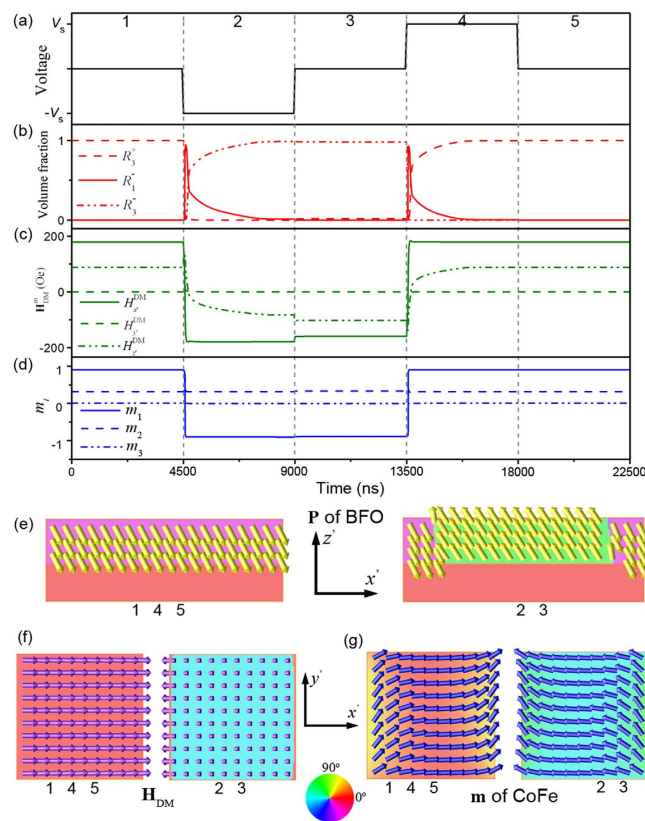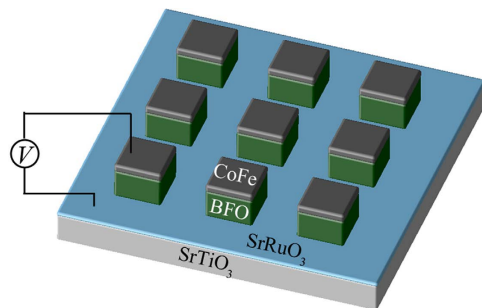
Figure 4. Polarization and magnetization dynamics in CoFe dot/(110)-BiFeO₃ film under voltage.
(**a**) Perpendicular voltage pulse applied on the poly-dot CoFe/(110)-thin-film BFO multiferroic heterostructure. (**b**) Voltage pulses induced ferroelectric phase evolutions of R_3^+, R_3^-, R_1^+, and R_1^- in BFO thin-film layer. (**c**) Voltage pulses induced interfacial $\mathbf{H}_{DM}$ field and hence (**d**) the magnetization evolution in CoFe dots. Voltage-induced corresponding (**e**) polarization domain-vector morphology in x'-z' middle cross-sectional plane of BFO-substrate layers, (**f**) the $\mathbf{H}_{DM}^m$, and (**g**) magnetization domain-vector morphologies in x'-y' plane middle cross-sectional plane of CoFe layer, respectively. The color wheel indicates the $\mathbf{P}$, $\mathbf{H}_{DM}^m$, or $\mathbf{m}$ orientation in the their correspondingly exhibited planes.

Figure 4 further shows the evolution of the distributions of polarization, interface $\mathbf{H}_{DM}$ field, and magnetization under successive square-wave bipolar voltage pulses with a constant duration of 4500 ns (Fig. 4a) in the CoFe dot (192 nm × 192 nm × 2.5 nm)/(110) BFO heterostrucuture. As it can be seen, non-volatile behaviors are exhibited for the 180° ferroelectric reversal (Fig. 4b,e) and subsequent reversal of the interface $\mathbf{H}_{DM}$ field from $[20\sqrt{2}]_{x'}$ to $[\overline{2}0\overline{\sqrt{2}}]_{x'}$ (see Fig. 4c,f). As a result, the in-plane magnetization component $m_{x'}$ can be reversed back and forth between the bistable states of −0.9 and 0.9 (i.e., a 150° reversal, see Fig. 4d,g) under perpendicular voltage. Moreover, as the magnetization switching (~75 ns) in the CoFe dot is much faster than the ferroelectric switching (~4500 ns) in the BFO thin film, the ferroelectric switching is the time-determining step during such perpendicular voltage-induced magnetization reversal.

The entire time of reversal, however, can be reduced by cutting out the continuous (110) BFO thin film into isolated islands so that the overlaying CoFe dot covers the whole surface of BFO (see Fig. 5). In this case, the polarization time can be greatly reduced because of the significantly released elastic energy. As demonstrated in Fig. 6, upon a negative voltage pulse of 495 ns (see the second stage of Fig. 6a), a single-domain 109° polarization switching from R_3^+ to R_1^- happens (Fig. 6b,e), leading to a reversal of the in-plane component of interface $\mathbf{H}_{DM}$ field from $[20\sqrt{2}]_{x'}$ to $[\overline{2}0\sqrt{2}]_{x'}$ (Fig. 6c,f). A similar 150° reversal of in-plane net magnetization occurs accordingly (Fig. 6d,g). Note that the time of 109° polarization switching is about 45 ns, which is the same as the magnetization switching time of 45 ns. As a result, the overall magnetization switching time driven by the perpendicular voltage is also 45 ns, which is about 100 times faster than the case in the heterostructures involving BiFeO₃ thin films (i.e., about 4500 ns as shown in Fig. 4).

Another advantage of using BiFeO₃ island based heterostructure is the significantly improved non-volatility (and thermal stability). Unlike the case of a continuous BFO thin film where the 180° domain wall between the poled region (R_3^-) and the unpoled region (R_3^+) leads to high electric energy,

Figure 5. Patterned CoFe/BiFeO$_3$ island heterostructure. Dot CoFe/(110)-island BFO multiferroic heterostructures grown on (110) SrTiO$_3$ substrate with CoFe and SrRuO$_3$ as the top and bottom electrodes, respectively.
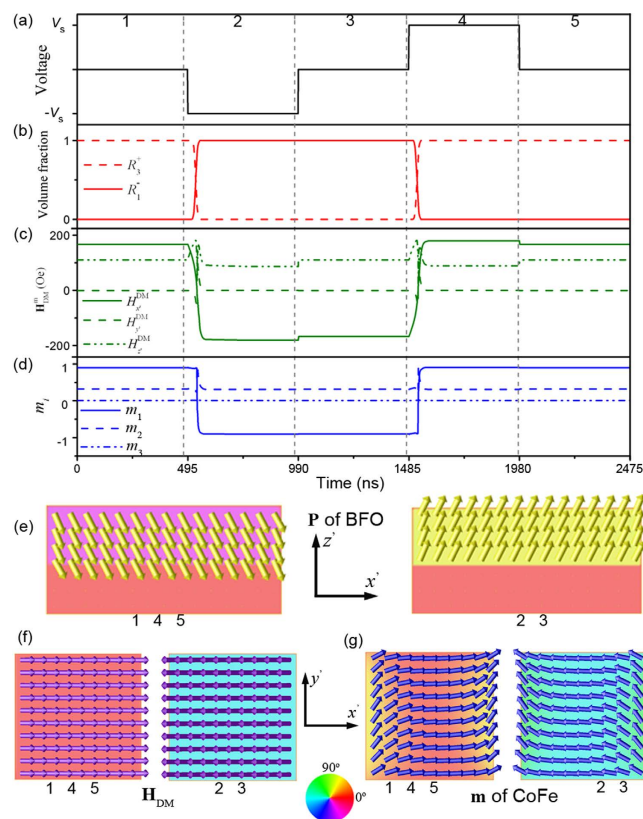
Figure 6. Polarization and magnetization dynamics in CoFe dot/(110)-BiFeO$_3$ island under voltage. (**a**) Perpendicular voltage pulse applied on the poly-dot CoFe/(110)-island BFO multiferroic heterostructure. (**b**) Voltage pulses induced ferroelectric phase evolutions of R_3^+ and R_1^- in BFO island layer. (**c**) Voltage pulses induced interfacial $\mathbf{H}_{DM}$ field and hence (**d**) the magnetization evolution in CoFe dots. Voltage-induced corresponding (**e**) polarization domain-vector morphology in x'-z' middle cross-sectional plane of BFO-substrate layers, (**f**) the $\mathbf{H}_{DM}^m$, and (**g**) magnetization domain-vector morphologies in x'-y' plane middle cross-sectional plane of CoFe layer, respectively. The color wheel indicates the $\mathbf{P}$, $\mathbf{H}_{DM}^m$, or $\mathbf{m}$ orientation in the their correspondingly exhibited planes.

the 109° switching in the present single-domain BFO island (Fig. 6b) is thermodynamically stable. Figure 7a shows the total free energy density profile of a single-domain BFO island by assuming the polarization pointing along every direction in the x'y'z' coordinate system. As it can be seen, R_1^+, R_3^+, R_1^-, and R_3^- are thermodynamically degenerate with equal depth at equilibrium states. The barrier (Δf) between R_1^+ and R_3^+ or R_1^- and R_3^- determines the stability of polarization under thermal fluctuation. For the CoFe dot only with in-plane magnetization, the energy barrier Δf between the global energy
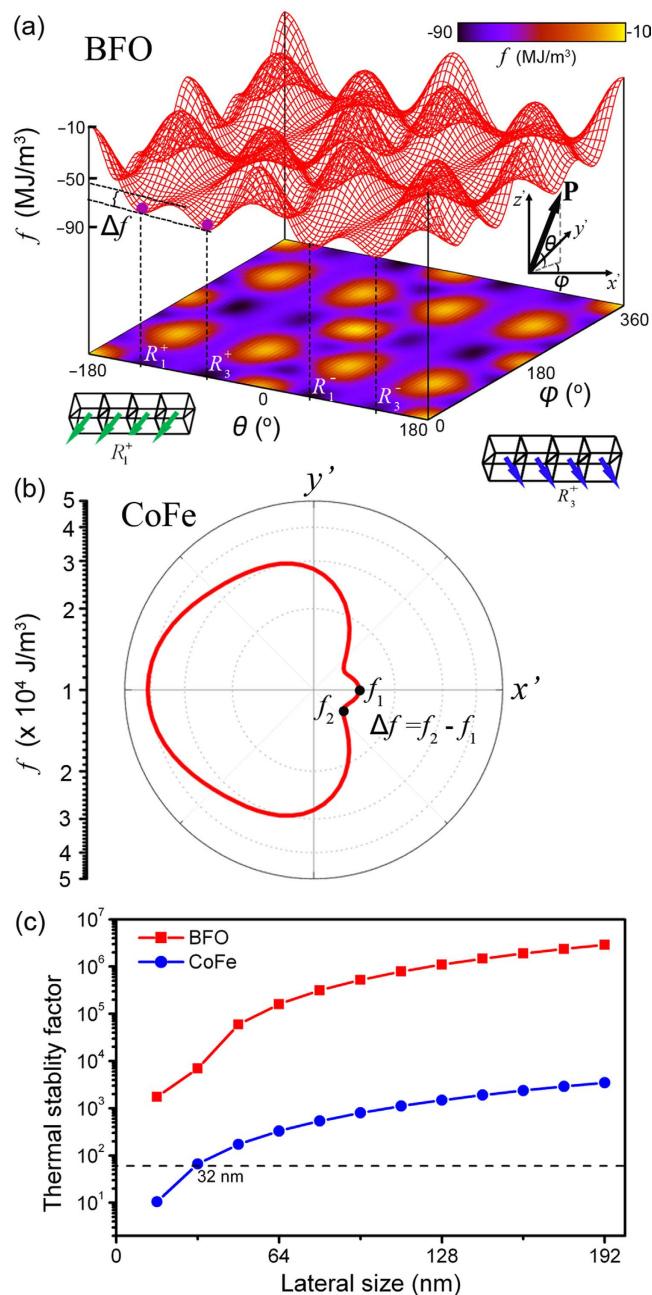
Figure 7. Thermal stability analysis in CoFe dot/(110)-BiFeO₃ island. (**a**) Energy profile as function of polarization orientation for single-domain BFO islands. (**b**) Energy polar plot for an in-plane magnetized CoFe dot with a size of 192 nm × 192 nm × 192 nm when the polarization in the bottom single-domain BFO island is along the R_3^+ direction. (**c**) Thermal stability factors as function of the respective lateral sizes (length and width) of BFO and CoFe. The thermal stability can be obtained from the energy profile by extracting the barrier (Δf) between the adjacent energy minimal.

minima at f_2 and the metastable state f_1 (induced by the interface $\mathbf{H}_{DM}$ field along the $[20\sqrt{2}]_{\mathbf{x}'}$ direction) determines the thermal stability of magnetization, as shown in Fig. 7b. Accordingly, the thermal stability factors of BFO island and CoFe dot can be calculated as $\Delta f \cdot V_i / (k_B T)$, where k_B and T are the Boltzmann constant and temperature in Kelvin, respectively, and V_i ($i =$ BFO, CoFe) is the volume.

    Figure 7c further shows the thermal stability factor of both BFO islands and CoFe dots as a function of their in-plane sizes, with their thicknesses fixed at 24 nm and 2.5 nm, respectively. As seen, the stability factors of the BFO islands are at least two orders of magnitude higher than those of the CoFe dots, indicating that the thermal stability of the heterostructure is determined by the latter. Such high thermal stability of polarization in single-domain BFO islands results from the high potential barrier between the

degenerate polarization states from the Landau-type bulk free energy. Nevertheless, the thermal stability factor of the CoFe dot can still be larger than 60 as its in-plane size exceeds $32\,nm \times 32\,nm$, suggesting a long timescale retention of magnetization states up to 10 years in the ideal case[39,40].

Discussion

In summary, perpendicular voltage-driven reversal of in-plane magnetization reversal has been demonstrated by phase-field simulations in multiferroic magnetoelectric heterostructures composed of polycrystalline CoFe dots and (110) BiFiO$_3$ continuous film or island. In the clamped BiFeO$_3$ thin film, the 180° ferroelectric reversal occurs by successive 109° and 71° ferroelastic switching. The non-volatility of such ferroelectric reversal can be enhanced by increasing the in-plane size of the overlaying CoFe dot, to alleviate the energy competition between the poled region underneath the CoFe dot and the rest region. Associated with repeatable polarization reversal, a repeatable 150° reversal of in-plane net magnetization reversal in the CoFe dot has been further demonstrated due to the reversal of the in-plane component of the interface H_{DM} field.

Similar non-volatile and repeatable voltage-induced magnetization reversal has been demonstrated when the BiFiO$_3$ thin film is etched into islands to release the substrate clamping and to eliminate the competition between the poled and unpoled regions. In such CoFe dot/BiFeO$_3$ island heterostructure, bistable 109° ferroelastic switching in single-domain BiFeO$_3$ has been demonstrated, which leads to 100 times faster ferroelectric switching (and hence faster overall response). As the switching time is estimated according to the Kolmogorov–Avrami–Ishibashi model (see Methods) which assumes that the polarization reversal occurs by domain wall nucleation and propagation, the calculated time (Fig. 6) for uniform switching in the CoFe dot/BiFeO$_3$ island heterostructure could be overestimated, i.e., the actual switching speed could be faster in the CoFe dot/BiFeO$_3$ island heterostructure, since we used the same value of the kinetic coefficient L in the TDGL equation for the BiFeO$_3$ island as for the BiFeO$_3$ thin film due to unknown for the island. Actually, the L values are different for continuous thin film and isolated island due to their different strain conditions, and should be larger in the BiFeO$_3$ island than in the clamped continuous thin film. A larger L in the BiFeO$_3$ island would yield a higher switching speed, though it is hard to estimate the actual switching speed in the island at present. Furthermore, the island heterostructure also shows good thermal stability even when the in-plane size of the heterostructure decreases down to $32\,nm \times 32\,nm$. These predictions would provide further directions for experimental studies of the BiFeO$_3$-based multiferroic heterostructures for potential spintronic device applications.

Methods

Phase-field model. In phase field modeling of the magnetic/BFO multiferroic heterostructures, the spatial distributions of local polarization and magnetization vectors are used to describe the ferroelectric and ferromagnetic domain structures, respectively. As the ferroelectric phase of BiFeO$_3$ has a rhombohedrally distorted perovskite structure with space group $R3c$, the spontaneous polarization of BiFeO$_3$ is along the pseudocubic $<111>_c$ in coordinate system xyz with x, y, and z along the $[100]_c$, $[010]_c$, and $[001]_c$ directions, respectively, giving rise to the formation of eight possible polarization variants, i.e., $R_1^+ = [\bar{1}\bar{1}\bar{1}]_c$, $R_2^+ = [\bar{1}11]_c$, $R_3^+ = [\bar{1}\bar{1}1]_c$, $R_4^+ = [1\bar{1}1]_c$, $R_1^- = [111]_c$, $R_2^- = [1\bar{1}\bar{1}]_c$, $R_3^- = [11\bar{1}]_c$, $R_4^- = [\bar{1}1\bar{1}]_c$ (see Fig. 1). For studying the ferroelectric domain structure in (110) BFO thin films, we introduce another coordinate system $x'y'z'$ with x', y', z' along the $[001]$, $[1\bar{1}0]$, and $[110]$ directions (see Fig. 1a). The polarization vector $\mathbf{P}'$ in the $x'y'z'$ coordinate system is chosen to be evolved by the time-dependent Landau-Ginzburg (TDGL) equation[41], i.e.,

$$\frac{\partial P_i'(\mathbf{r}, t)}{\partial t} = -L\frac{\delta F_P}{\delta P_i'(\mathbf{r}, t)}, \tag{1}$$

where L the kinetic coefficient related to the domain wall mobility and F_P the total free energy of the FE layer, respectively. The total free energy of the FE layer includes the bulk, elastic, electric, and the gradient energies, i.e.,

$$F_P = \iiint_{V_P} \left(f_{bulk} + f_{elastic}^p + f_{electric} + f_{grad} \right) dV, \tag{2}$$

where V_P represents the volume of the FE layer in the heterostructure.

The expressions for the bulk, elastic, electric, and gradient energy densities were used as before[41–43]. The correspondence of the polarization components P_j in coordinate system xyz to the counterparts P_i' in $x'y'z'$ is $P_i' = T_{ij}P_j$ with T_{ij} the transformation matrix given as follows:

$$T_{ij} = \begin{pmatrix} 0 & 0 & 1 \\ -1/\sqrt{2} & 1/\sqrt{2} & 0 \\ 1/\sqrt{2} & 1/\sqrt{2} & 0 \end{pmatrix}. \tag{3}$$

Note that when calculating the elastic, electric, and gradient energy densities, the related tensors including the electrostrictive coefficient tensor, background dielectric constant tensor, gradient energy coefficient tensor have to be performed transformation from coordinate system xyz to the $x'y'z'$ (see Ref. 41). For solving the mechanical equilibrium equation, Khachaturyan's microelastic theory[44] is employed by incorporating the thin-film[45] or the isolated-island[43,46] boundary conditions for the cases of BFO continuous film and island, respectively. For (110) BFO film grown on (110) SrTiO$_3$ substrate under full constraint, the film/substrate mismatch strain e_{ij}^s are $e_{11}^s = e_{22}^s = -1.26\%$ and $e_{12}^s = e_{21}^s = 0$[47,48].

For solving the electrostatic equilibrium equation, the Fast Fourier Transformation method is employed by incorporating the short-circuit surface boundary condition[49] through which the externally applied voltage on BFO by CoFe and SrRuO$_3$ bottom electrode is introduced into the phase field model.

For determining the real time scale corresponding to each iteration step of the TDGL equation, the switching dynamics as a function of iteration step is obtained and compared to the Kolmogorov–Avrami–Ishibashi (KAI) model[50,51] as following

$$P(t) = 2P_S\{1 - \exp[-(t/t_0)^n]\}, \tag{4}$$

where $P(t)$ the switched polarization, t the real time, P_S the saturated polarization, t_0 the characteristic switching time, and n the effective dimension of domain growth. For (110) BFO thin film, n has a value of 2 and t_0 is about 1.5×10^{-7}s with the applied electric field of $250\,\text{kV/cm}$[34]. Our simulation shows that a real time interval of $\Delta t = 8.25 \times 10^{-10}$s for the polarization domain evolution is determined corresponding to the each iteration step of TDGL equation.

The evolution of the magnetic domain structures of the FM layer can be described by the Landau-Lifshitz-Gilbert (LLG) equation, i.e.,

$$(1 + \alpha^2)\frac{\partial \mathbf{M}}{\partial \tau} = -\gamma_0 \mathbf{M} \times \mathbf{H}_{\text{eff}} - \frac{\gamma_0 \alpha}{M_S} \mathbf{M} \times (\mathbf{M} \times \mathbf{H}_{\text{eff}}), \tag{5}$$

where γ_0 the gyromagnetic ratio and α the Gilbert damping constant, respectively. The real time interval for the magnetic domain evolution determined by $\Delta\tau(1+\alpha^2)/(\gamma_0 M_s)$ corresponding to each iteration step of Eq. (5) is about 0.06 ps with $\gamma_0 = -2.2 \times 10^5 \text{m} \cdot \text{A}^{-1} \cdot \text{s}^{-1}$ (from Ref. 52), $\alpha = 0.01$ (from Ref. 32), and $\Delta\tau = 0.02$. $\mathbf{H}_{\text{eff}}$ is the effective magnetic field, given as $\mathbf{H}_{\text{eff}} = -(1/\mu_0)(\delta F_\text{m}/\delta\mathbf{M})$, with μ_0 denoting the vacuum permeability and F_m the total free energy of the CoFe layer. The F_m is formulated as,

$$F_M = \iiint_V \left(f_{\text{anis}} + f_{\text{exch}} + f_{\text{ms}} + f_H + f_{\text{elastic}}^\text{m}\right)dV, \tag{6}$$

where f_{anis}, f_{exch}, f_{ms}, f_H, and $f_{\text{elastic}}^\text{m}$ the magnetocrystalline anisotropy, exchange, magnetostatic, the $\mathbf{H}_{\text{DM}}$-field, and elastic energy densities, respectively. Regarding that the CoFe layer is grown in isotropically polycrystalline or amorphous states, all the above energy density expressions are independent of the coordinate system. Among them, the f_{anis} is neglected for simplicity due to the isotropic nature of the polycrystalline film. The isotropic f_{exch} is determined by the gradient of local magnetization vectors, i.e.,

$$f_{\text{exch}} = J[(\nabla m_1)^2 + (\nabla m_2)^2 + (\nabla m_3)^2], \tag{7}$$

where J denotes the exchange stiffness constant. The magnetostatic energy density f_{ms} can be written as,

$$f_{\text{ms}} = -\frac{1}{2}\mu_0 M_S(\mathbf{H}_d \cdot \mathbf{m}). \tag{8}$$

Here $\mathbf{H}_d$ denotes the stray field, and it can be numerically calculated by employing a finite-size magnetostatic boundary condition previously developed for a 3D array of ferromagnetic cubes[53].

For the $\mathbf{H}_{\text{DM}}$-field induced energy density, it is similar to the Zeeman energy of an external magnetic field, and can be expressed as

$$f_H = -\mu_0 M_S(\mathbf{H}_{\text{DM}}^\text{m} \cdot \mathbf{m}). \tag{9}$$

Here the $\mathbf{H}_{\text{DM}}^\text{m}$ indicates the $\mathbf{H}_{\text{DM}}$-field that penetrates onto the CoFe film through the interface, and is given by,

$$\mathbf{H}_{\text{DM}}^\text{m} = \frac{1}{t_i}\int_{t_i}\mathbf{H}_{\text{DM}}'dz, \tag{10}$$

where t_i denotes the thickness of the interface creating interfacial magnetic interaction, and the $\mathbf{H}_{\text{DM}}'$ represents the $\mathbf{H}_{\text{DM}}$-field vector in the BFO layer in coordinate system $x'y'z'$. $\mathbf{H}_{\text{DM}}'$ can be obtained from $\mathbf{H}_{\text{DM}}$ using coordinate transformation $\mathbf{H}_{\text{DM}}' = \mathbf{T}\mathbf{H}_{\text{DM}}$, wherein the $\mathbf{H}_{\text{DM}}$ can be obtained through $\mathbf{H}_{\text{DM}} = \mathbf{P} \times \mathbf{L}$. With regard to the antiferromagnetic vector $\mathbf{L}$, it was predicted with a sixfold degeneracy

in bulk BiFeO$_3$ system. However, in thin-film system, this sixfold degeneracy is broken and only one easy axis remains, according to the experimental observations and first-principle calculations[33]. Therefore, the preserved antiferromagnetic vector **L** coinciding with **P** for thin-film BiFeO$_3$ in *xyz* coordinate system can be phenomenologically described by

$$\mathbf{L} = \begin{cases} (|P_2|, \; -|P_1|, \; 0), \; (P_1 P_2 > 0) \\ (|P_2|, \; |P_1|, \; 0), \; (P_1 P_2 < 0) \end{cases} \tag{11}$$

or the correspondingly equivalent directions. From Eq. (11) one can see that the antiferromagnetic vector **L** remains for the perpendicular 71° and 180° polarization switching under perpendicular voltage, while it rotates 90° for the in-plane 71° polarization switching under in-plane voltage in (001) BiFeO$_3$ thin films, in consistent with the experimental results[13,33]. Thus, the DM effect induced **H**$_{DM}$ field can be written as

$$\mathbf{H}_{DM} = \mathbf{P} \times \mathbf{L} = h_{DM}^0 \left(\frac{P_1}{|\mathbf{P}|}, \; \frac{P_2}{|\mathbf{P}|}, \; \frac{P_3}{|\mathbf{P}|} \right) \times \left(\frac{L_1}{|\mathbf{L}|}, \; \frac{L_2}{|\mathbf{L}|}, \; \frac{L_3}{|\mathbf{L}|} \right)$$

$$= \frac{h_{DM}^0}{\sqrt{(P_1^2 + P_2^2 + P_3^2)(P_1^2 + P_2^2)}}$$

$$\begin{cases} (|P_1|P_3 \quad |P_2|P_3, \; -|P_1|P_1 \; -|P_2|P_2),(P_1 P_2 > 0) \\ (-|P_1|P_3, \; |P_2|P_3, \; |P_1|P_1, \; -|P_2|P_2),(P_1 P_2 < 0) \end{cases}. \tag{12}$$

The P_i and L_i ($i = 1,2,3$) are the components of the polarization vectors and the antiferromagnetic vectors in coordinate system *xyz*, and the h_{DM}^0 represents the magnitude of the **H**$_{DM}$ field. Note that the expression of **H**$_{DM}$ field published in our previous paper is just a specific case for studying the in-plane 71° polarization switching in (001) BiFeO$_3$ thin film[13]. Equation (12) clearly indicates that **P**-dependent nature of the **H**$_{DM}$ field related to individual ferroelectric domain at the BFO surface, which can propagate across the hetero-interface and act on the CoFe dots. Combining Eqs. (3) and (12), Eq. (10) can be rewritten as,

$$H_{DM}^m =$$

$$\begin{cases} \dfrac{h_{DM}^0}{t_i} \displaystyle\int_{t_i} \dfrac{(-|P_1|P_1 - |P_2|P_2, \; (-|P_1|P_3 + |P_2|P_3)/\sqrt{2}, \; (|P_1|P_3 + |P_2|P_3)/\sqrt{2})}{\sqrt{(P_1^2 + P_2^2 + P_3^2)(P_1^2 + P_2^2)}} dz \\[2mm] \qquad , \; (P_1 P_2 > 0) \\[2mm] \dfrac{h_{DM}^0}{t_i} \displaystyle\int_{t_i} \dfrac{(|P_1|P_1 - |P_2|P_2, \; (|P_1|P_3 + |P_2|P_3)/\sqrt{2}, \; (-|P_1|P_3 + |P_2|P_3)/\sqrt{2})}{\sqrt{(P_1^2 + P_2^2 + P_3^2)(P_1^2 + P_2^2)}} dz, \\[2mm] \qquad (P_1 P_2 < 0) \end{cases}. \tag{13}$$

The formulation of the elastic energy density $f_{elastic}^m$ of CoFe layer is also same as before[16]. Note that for a (110) BFO film under perpendicular voltage approaching to saturation the in-plane ferroelastic strain remains unchanged whenever the polarization vector is up or down, thus only the structural strain introduced during growth of CoFe is affecting the initial magnetization.

Temporal evolutions of the ferroelectric and magnetic domain structures are obtained by numerically solving the TDGL and LLG equations using semi-implicit Fourier spectral method and Gauss-Seidel projection method, respectively. The material parameters used for simulations, including the Landau coefficients, electrostrictive coefficients, elastic constants of BFO layer, and the saturated magnetization, exchange stiffness constant, elastic constants of CoFe layer can be found in the literature[16,41,54] and are listed as following: $\alpha_1 = 4.9(T - 1103) \times 10^5 \text{C}^{-2}\text{m}^2\text{N}$ (where the temperature T is in K), $\alpha_{11} = 5.42 \times 10^8 \text{C}^{-4}\text{m}^6\text{N}$, $\alpha_{12} = 1.54 \times 10^8 \text{C}^{-4}\text{m}^6\text{N}$, $Q_{1111} = 0.032\text{C}^{-2}\text{m}^4$, $Q_{1122} = -0.016\text{C}^{-2}\text{m}^4$, $Q_{1212} = 0.06\text{C}^{-2}\text{m}^4$, $c_{1111}^p = 3.02 \times 10^{11} \text{Nm}^{-2}$, $c_{1122}^p = 1.62 \times 10^{11} \text{Nm}^{-2}$, $c_{1212}^p = 0.68 \times 10^{11} \text{Nm}^{-2}$; For isotropically amorphous CoFe film, $M_S = 1.59 \times 10^6 \text{Am}^{-1}$, $J = 3.0 \times 10^{11} \text{Jm}^{-1}$, $c_{1111}^m = 2.77 \times 10^{11} \text{Nm}^{-2}$, $c_{1122}^m = 1.28 \times 10^{11} \text{Nm}^{-2}$, $c_{1212}^m = (c_{1111}^m - c_{1122}^m)/2$. The discrete grid points of $128\Delta x \times 128\Delta y \times 48\Delta z$ with real grid space $\Delta x = \Delta y = \Delta z = 1$ nm are employed to describe the BFO film/substrate system, wherein the thickness of BFO t_p is taken as 24 nm by setting $t_p = 24\Delta z$, and the thickness of the interface t_i creating the interfacial magnetic interaction is assigned a value of 4 nm by

setting $t_i = 4\Delta z$. While for CoFe dots, discrete grid points of $N\Delta x \times N\Delta y \times 20\Delta z$ with $\Delta x = \Delta y = 1$ nm, and $\Delta z = 0.5$ nm are used, where the thickness of the CoFe t_m is set to be 2.5 nm by taking $t_m = 5\Delta z$ and the in-plane size $N\Delta x$ can be given by setting N. When the in-plane size of CoFe layer is larger than 96×96 nm^2, the real size of the heterostructure is achieved by changing Δx and Δy but keeping $N = 96$. For the BFO island, the discrete grid points of $128\Delta x \times 128\Delta y \times 48\Delta z$ with real grid space $\Delta x = \Delta y = 2$ nm and $\Delta z = 1$ nm are employed with $N\Delta x \times N\Delta y \times 24\Delta z$ of them are occupied by the BFO island while the rest are the air which allows the lateral relaxation of the island.

References

1. Eerenstein, W., Mathur, N. D. & Scott, J. F. Multiferroic and magnetoelectric materials. *Nature* **442,** 759 (2006).
2. Duan, C. G., Jaswal, S. S. & Tsymbal, E. Y. Predicted magnetoelectric effect in Fe/BaTiO₃ multilayers: ferroelectric control of magnetism. *Phys. Rev. Lett.* **97,** 047201 (2006).
3. Vaz, C. A. F. Electric field control of magnetism in multiferroic heterostructures. *J. Phys: Condens. Matter* **24,** 333201 (2012).
4. Cuellar, F. A. *et al.* Reversible electric-field control of magnetization at oxide interfaces. *Nature Commun.* **5,** 4215 (2014).
5. Garcia, V. *et al.* Ferroelectric control of spin polarization. *Science* **327,** 1106 (2010).
6. Ramesh, R. & Spaldin, N. Multiferroics: progress and prospects in thin films. *Nature Mater.* **6,** 21 (2007).
7. Vaz, C. A. F., Hoffman, J., Ahn, C. H. & Ramesh, R. Magnetoelectric coupling effects in multiferroic complex oxide composite structures. *Adv. Mater.* **22,** 2900 (2010).
8. Ma, J., Hu, J. M., Li, Z. & Nan, C. W. Recent progress in multiferroic magnetoelectric composites: from bulk to thin films. *Adv. Mater.* **23,** 1062 (2011).
9. Chu, Y. H., Martin, L. W., Holcomb, M. B. & Ramesh, R. Controlling magnetism with multiferroics. *Mater. Today* **10,** 16 (2007).
10. Chu, Y.-H. *et al.* Electric-field control of local ferromagnetism using a magnetoelectric multiferroic. *Nat. Mater.* **7,** 478–482 (2008).
11. Lebeugle, D., Mougin, A., Viret, M., Colson, D. & Ranno, L. Electric field switching of the magnetic anisotropy of a ferromagnetic layer exchange coupled to the multiferroic compound BiFeO₃. *Phys. Rev. Lett.* **103,** 257601 (2009).
12. Wu, S. M. *et al.* Reversible electric control of exchange bias in a multiferroic field-effect device. *Nat. Mater.* **9,** 756 (2010).
13. Heron, J. *et al.* Electric-field-induced magnetization reversal in a ferromagnet-multiferroic heterostructure. *Phys. Rev. Lett.* **107,** 217202 (2011).
14. Huijben, M., Yu, P., Martin, L. W., Molegraaf, H. J., Chu, Y. H., Holcomb, M. B., Balke, N., Rijnders, G. & Ramesh, R. Ultrathin limit of exchange bias coupling at oxide multiferroic/ferromagnetic interfaces *Adv. Mater.* **25,** 4739 (2013).
15. Trassin, M. *et al.* Interfacial coupling in multiferroic/ferromagnet heterostructures. *Phys. Rev. B* **87,** 134426 (2013).
16. Wang, J. J., Hu, J.M., Yang, T. N., Feng, M., Zhang, J. X., Chen, L. Q. & Nan, C.W. Effect of strain on voltage-controlled magnetism in BiFeO₃-based heterostructures. *Sci. Rep.* **4,** 4553 (2014).
17. Hambe, M., Petraru, A., Pertsev, N. A., Munroe, P., Nagarajan, V. & Kohlstedt, H. Crossing an Interface: Ferroelectric control of tunnel currents in magnetic complex oxide heterostructures. *Adv. Funct. Mater.* **20,** 2436 (2010).
18. Rana, A., Lu, H., Bogle, D. K., Zhang, Q., Vasudevan, R., Thakare, V., Gruverman, A., Ogale, S. & Nagarajan, V. Scaling behavior of resistive switching in epitaxial bismuth ferrite heterostructures. *Adv. Funct. Mater.* **24,** 3962 (2014).
19. Hu, J. M., Li, Z., Chen, L.Q. & Nan, C. W. High-density magnetoresistive random access memory operating at ultralow voltage at room temperature. *Nature Commun.* **2,** 553 (2011)
20. Hu, J. M., Li, Z., Chen, L.Q. & Nan, C.W. Design of a voltage-controlled magnetic random access memory based on anisotropic magnetoresistance in a single magnetic layer. *Adv. Mater.* **24,** 2869 (2012).
21. Heron, J. *et al.* Deterministic switching of ferromagnetism at room temperature using an electric field. *Nature* **516,** 370 (2014).
22. Zhang, J. X., Li, Y. L., Schlom, D. G., Chen, L. Q., Zavaliche, F., Ramesh, R. & Jia, Q. X. Phase-field model for epitaxial ferroelectric and magnetic nanocomposite thin film. *Appl. Phys. Lett.* **90,** 052909 (2007).
23. Hu, J. M., Yang, T., Chen, L. & Nan, C. W. Voltage-driven perpendicular magnetic domain switching in multiferroic nanoislands. *J. Appl. Phys.* **113,** 194301 (2013).
24. Cruz, M. P., Chu, Y. H., Zhang, J. X., Yang, P. L., Zavaliche, F., He, Q., Shafer, P., Chen, L. Q. & Ramesh, R. Strain control of domain-wall stability in epitaxial BiFeO₃ (110) films. *Phys. Rev. Lett.* **99,** 217601 (2007).
25. Tseng, A. A. Recent developments in nanofabrication using ion projection lithography. *Small* **1,** 594 (2005).
26. Chu, Y. H., Cruz, M. P., Yang, C. H., Martin, L. W., Yang, P. L., Zhang, J. X., Lee, K., Yu, P., Chen, L. Q. & Ramesh, R. Domain control in multiferroic BiFeO₃ through substrate vicinality *Adv. Mater.* **19,** 2662 (2007).
27. Chu, Y. H. *et al.* Nanoscale domain control in multiferroic BiFeO₃ thin films *Adv. Mater.* **18,** 2307 (2006).
28. Dzyaloshinskii, I. E. Thermodynamic theory of 'weak' ferromagnetism in antiferromagnetic substances. *Sov. Phys. JETP* **5,** 1259 (1957).
29. Moriya, T. Anisotropic superexchange interaction and weak ferromagnetism *Phys. Rev.* **120,** 91 (1960).
30. Ederer, C. & Spaldin, N. A. Weak ferromagnetism and magnetoelectric coupling in bismuth ferrite. *Phys. Rev. B* **71,** 060401 (2005).
31. Ederer, C. & Fennie, C. J. Electric-field switchable magnetization via the Dzyaloshinskii–Moriya interaction: FeTiO₃ versus BiFeO₃. *J. Phys.: Condens. Matter* **20,** 434219 (2008).
32. Qiu, D., Ashraf, K. & Salahuddin, S. Nature of magnetic domains in an exchange coupled BiFeO₃/CoFe heterostructure. *Appl. Phys. Lett.* **102,** 112902 (2013).
33. Zhao, T., *et al.* Electrical control of antiferromagnetic domains inmultiferroic BiFeO₃ films at room temperature *Nature Mater.* **5,** 823(2006).
34. Pantel, D., Chu, Y. H., Martin, L. W., Ramesh, R., Hesse, D. & Alexe, M. Switching kinetics in epitaxial BiFeO₃ thin films. *J. Appl. Phys.* **107,** 084111(2010).
35. Gruverman, A., Wu, D. & Scott, J. F. Piezoresponse force microscopy studies of switching behavior of ferroelectric capacitors on a 100-ns time scale. *Phys. Rev. Lett.* **100,** 097601(2008).
36. Baek, S. H. *et al.* Ferroelastic switching for nanoscale non-volatile magnetoelectric devices *Nature Mater.* **9,** 309(2010).
37. Nelson, C. T. *et al.* Domain dynamics during ferroelectric switching. *Science* **334,** 968(2011).
38. Cowburn, R. P. & Welland M. E. Micromagnetics of the single-domain state of square ferromagnetic nanostructures. *Phys. Rev. B* **58,** 9217 (1998).
39. Zhu, J. G. Magnetoresistive random access memory: the path to competitiveness and scalability. *Proceedings of the IEEE* **96,** 1786 (2008).
40. Evans, R., Chantrell, R.W., Nowak, U., Lyberatos, A. & Richter, H. J. Thermally induced error: Density limit formagnetic data storage. *Appl. Phys. Lett.* **100,** 102402 (2012).

41. Zhang, J. X., Li, Y. L., Choudhury, S., Chen, L. Q., Chu, Y. H., Zavaliche, F., Cruz, M. P., Ramesh, R. & Jia, Q. X. Computer simulation of ferroelectric domain structures in epitaxial BiFeO$_3$ thin film. *J. Appl. Phys.* **103,** 094111 (2008).
42. Wang, J. J., Wu, P. P., Ma, X. Q. & Chen, L. Q. Temperature-pressure phase diagram and ferroelectric properties of BaTiO$_3$ single crystal based on a modified Landau potential. *J. Appl. Phys.* **108,** 114105 (2010).
43. Wang, J. J., Ma, X. Q., Li, Q., Britson, J. & Chen, L. Q. Phase transitions and domain structures of ferroelectric nanoparticles: Phase field model incorporating strong elastic and dielectric inhomogeneity. *Acta Mater.* **61,** 7591 (2013).
44. Khachaturyan, A. *Theory of structural transformations in solid.* (Wiley, 1983).
45. Li, Y. L., Hu, S. Y., Liu, Z. K. & Chen, L. Q. Effect of substrate constraint on the stability and evolution of ferroelectric domain structures in thin film. *Acta Mater.* **50,** 395 (2002).
46. Zhang, J. X., Wu, R., Choudhury, S., Li, Y. L., Hu, S. Y. & Chen, L. Q. Three-dimensional phase-field simulation of domain structures in ferroelectric islands. *Appl. Phys. Lett.* **92,** 122906 (2008).
47. Zavaliche, F., Yang, S. Y., Zhao, T., Chu, Y. H., Cruz, M. P., Eom, C. B. & Ramesh, R. Multiferroic BiFeO$_3$ films: domain structure and polarization dynamics. *Phase Transitions* **79,** 991 (2006).
48. Schlom, D. G., Chen, L. Q., Eom, C. B., Rabe, K. M., Streiffer, S. K. & Triscone, J. M. Strain tuning of ferroelectric thin films. *Annu. Rev. Mater. Res.* **37,** 589 (2007).
49. Li, Y. L., Hu, S. Y., Liu, Z. K. & Chen, L. Q. Effect of electrical boundary conditions on ferroelectric domain structures in thin film. *Appl. Phys. Lett.* **81,** 427 (2002).
50. Ishibashi, Y. & Takagi, Y. Note on ferroelectric domain switching. *J. Phys. Soc. Jpn.* **31,** 506 (1971).
51. Ishibashi, Y. Polarization reversal kinetics in ferroelectric liquid crystals. *Jpn. J. Appl. Phys.* Part 1 **24,**126 (1985).
52. Walowski, J., Kaufmann, M. D., Lenk, B., Hamann, C., McCord, J. & Münzenberg, M. Intrinsic and non-local Gilbert damping in polycrystalline nickel studied by Ti : sapphire laser fs spectroscopy. *J. Phys. D: Appl. Phys.* **41,**164016 (2008).
53. Schabes, M. E. & Aharoni, A. Magnetostatic interaction fields for a three-dimensional array of ferromagnetic cubes. *IEEE Trans. Magn.* **23,** 3882 (1987).
54. Hall, R. C. Magnetic anisotropy and magnetostriction of ordered and disordered cobalt-iron alloys. *J. Appl. Phys.* **31,** S157 (1960).

Acknowledgements

Author Contributions

J.J.W., J.M.H. and P.R.C. performed the simulations. C.W.N. and L.Q.C. directed the work. J.J.W., J.M.H., and C.W.N. co-wrote the paper. J.J.W., J.M.H., Y.G., Y.S., L.Q.C. and C.W.N analyzed the data. All contributed discussion.

Additional Information

Competing financial interests: The authors declare no competing financial interests.

How to cite this article: Wang, J. J. *et al.* Magnetization Reversal by Out-of-plane Voltage in BiFeO$_3$-based Multiferroic Heterostructures. *Sci. Rep.* **5**, 10459; doi: 10.1038/srep10459 (2015).

SCIENTIFIC REP♥RTS

OPEN **Corrigendum:** Magnetization Reversal by Out-of-plane Voltage in BiFeO₃-based Multiferroic Heterostructures

J. J. Wang, J. M. Hu, Ren-Ci Peng, Y. Gao, Y. Shen, L. Q. Chen & C. W. Nan

This Article contains a typographical error in a grant number in the Acknowledgements section.